Justine Kemp ORCID iD: 0000-0003-0472-6960

# A multi-method approach to dating the burial and skeleton of Kiacatoo Man, New South Wales, Australia

Timothy Pietsch[a], Justine Kemp[a], Colin Pardoe[b], Rainer Grün[a], Jon Olley[a], Rachel Wood[b]

[a] Australian Rivers Institute, Griffith University, Nathan, Queensland 4111

[b] Department of Archaeology and Natural History, The Australian National University, Canberra 0200

Timothy Pietsch*

Australian Rivers Institute, Griffith University, Nathan, Queensland, Australia 4111; t.pietsch@griffith.edu.au

Justine Kemp

Australian Rivers Institute, Griffith University, Nathan, Queensland, Australia 4111; j.kemp@griffith.edu.au

Colin Pardoe

Department of Archaeology and Natural History, The Australian National University, Canberra, Australian Capital Territory, Australia 0200; colin.pardoe@ozemail.com.au

Rainer Grün

This is the author manuscript accepted for publication and undergone full peer review but has not been through the copyediting, typesetting, pagination and proofreading process, which may lead to differences between this version and the Version of Record. Please cite this article as doi: 10.1002/jqs.3165.

Research School of Earth Sciences, The Australian National University, Canberra, Australian Capital Territory, Australia 0200; r.grun@griffith.edu.au

Jon Olley

Australian Rivers Institute, Griffith University, Nathan, Queensland, Australia 4111; j.olley@griffith.edu.au

Rachel Wood

Research School of Earth Sciences, The Australian National University, Canberra, Australian Capital Territory, Australia 0200; rachel.wood@anu.edu.au

*corresponding author

**Keywords**: archaeology; quartz OSL; luminescence dating; U-series; Wiradjuri

Abstract

Kiacatoo Man, a large, rugged Aboriginal adult buried in the Lachlan riverine plains, southeastern Australia, was discovered in 2011. Laser-ablation uranium series analysis on bone yielded a minimum age for the burial of 27.4 ± 0.4 ka (2σ). Single-grain, optically stimulated luminescence ages on quartz sediment in which the grave had been dug gave a weighted mean age of 26.4 ± 1.5 ka (1σ). Luminescence samples from the grave infill and from sediment beneath the grave exhibit overdispersed dose distributions consistent with bioturbation or other disturbance, which has obscured the burial signal. The overlap between the minimum (U-series) and maximum (luminescence) ages places the burial between 27.0 ka and 29.4 ka (2σ). Luminescence ages obtained from the channel belt of between 28 ± 2 ka and 25 ± 3 ka indicate that fluvial sedimentation was occurring prior to the Last Glacial Maximum, which is consistent with the broader geomorphic setting. Together, these results are internally and regionally consistent, and indicate that Kiacatoo Man was one of the more ancient individuals so far identified in Australia. His remains are important to our understanding of patterns of biological variation and other processes that have shaped people in the Murray-Darling Basin through time.

## Introduction

The discovery of ancient human burials affords the opportunity to observe directly the interplay of people and their environment, with grave-held skeletal remains providing both physical and cultural evidence of ancient societies. In Australia, the patterns of human occupation and their relationship to environmental changes through the late Quaternary have been the basis of significant research effort (e.g. Bowler, 1998; Stern et al., 2013; Hill and Durband, 2014; Long et al., 2014; Fitzsimmons et al., 2014, 2015; Stern, 2015; Pardoe, 1990, 1995, 2006, 2010). The dating of ancient human remains has been particularly problematic owing to the long timespan of modern human occupation of the continent, poor preservation of organic remains, mistaken stratigraphic associations (Pardoe, 1993; Gillespie, 1998), and the open system behaviour of uranium and other limitations inherent in the dating techniques (Thorne et al., 1999; Bowler and Magee, 2000; Gillespie and Roberts, 2000; Grün et al., 2000; Bowler et al., 2003).

In 2011, erosion of a natural levee associated with an ancient channel belt of the Lachlan River in central New South Wales revealed a human burial (Fig. 1A, 2), with initial investigations of exposed cranial fragments indicating them to be non-European and of some antiquity (Kemp et al., 2014a). This is also a key individual to Wiradjuri descendants, relating them to their ancient neighbours downstream at the Willandra Lakes. The burial was exposed by heavy rain in the surface of a disused vehicle track with damage to the skeleton associated with vehicular traffic and stock trampling: the slightly higher elevation of the levee is a position favoured by stock, and the burial was also located near a gate and feed silo. The environmental setting of the burial site and a brief description of the remains provide background to our attempts to determine its age using uranium- (U) series and radiocarbon ($^{14}$C) dating of bone, and

single-grain, optically stimulated luminescence (OSL) dating of the grave infill sediments, the underlying levee and associated palaeochannel sediments.

## Environmental setting and skeletal morphology

The burial site is located on a low (<~1 m) linear rise that forms the northern boundary of an ancient channel belt on the Lachlan riverine plains near Kiacatoo in central New South Wales (33.04 °S, 146.72 °E – Fig 1A, 1B). Field investigation revealed this feature to be a natural levee characterised by pale reddish brown and strong brown silty fine sand (Kemp et al., 2014a). The levee varies between ~100 m and ~300 m in width and can be traced on aerial photographs for several kilometres either side of the modern Lachlan River. Lateral migration within the previously undescribed channel belt associated with the levee produced the arcuate patterns in the levee that closely follows its northern boundary (Fig. 1C). The levee surface was searched for artefacts, with ground penetrating radar transects adjacent to Kiacatoo Man indicating potential additional burial sites (Kemp et al., 2014a).

The burial was excavated in May 2011. A preliminary description of the skeleton is provided in Kemp et al. (2014). Only fragments of the cranium remained along with the right mandibular body. The post-cranial skeleton was complete, but fragmented with poor preservation of articular surfaces and other elements with thinner cortical bone (Fig. 2B). Very little cancellous, or spongy, bone was preserved. The bone was evenly mineralised, but with slightly darker colouration on the external surfaces. No chemical examination of the mineralisation was possible. Manganese staining was not evident. A carbonate wash was present over exposed surfaces and appeared to be of an even thickness on upper and lower surfaces of the bone in resting position. The carbonate had infiltrated the bone, assisting the destruction of cancellous bone and

exacerbating or causing expansion of micro-fractures so that, while complete, much of the skeleton was fragmented before excavation. Given the greater amount of carbonate on external surfaces compared to broken edges, it may be that vehicular traffic was responsible for a considerable part of the fracturing. Denser cortical bones, such as central femur and tibia and mandibular body, were better preserved. Despite the fragmentation, a limited reconstruction was possible during excavation and in the time the remains were in the laboratory. Measurements of wrist, thigh and skull indicate an individual of considerable size and rugosity, placing him in the uppermost percentiles for body size for people in Australia (Pardoe, 1995, 2010).

## Methods

### Field methods

The general environs of the burial site were investigated over ~2 $km^2$ and major landform features were mapped from satellite imagery (Fig. 1C). Sub-surface sediments of the levee were described from cores extracted with a hand-auger at depths of 1 m, 2 m and 4 m, 30 m west of the burial site, and from the medium and coarse sandy bed of the adjacent palaeochannel, 215 m west at 4.6 m depth. The skeleton was excavated first by cutting a side trench along the grave margin (Fig. 2A). Samples for OSL dating were collected from grave infill amidst the skeletal remains, and from sediments immediately below the grave boundary as identified in the field (Fig. 2). The grave boundary was apparent as a weak change in soil pedal structure ~0.15 m below the present-day surface. The sampling design reflected our expectation that grave infill sediments would post-date the age of the levee sediments into which the grave had been cut. In the trench, five OSL sample tubes were inserted horizontally above and below the grave boundary (Fig. 1B, 2). A sixth sample tube was inserted vertically behind the thorax from the partly excavated surface. The

skeleton was then excavated from the side trench, minimising damage caused by removal of the hard soil. Skeletal elements were bagged separately where possible, but the fragility of the axial skeleton was such that it was removed in three blocks, allowing for cleaning in the laboratory. The skeletal remains were described and subsampled for radiocarbon and U-series analysis, and were collected by Wiradjuri representatives on behalf of Aboriginal groups, namely Murrin Bridge, West Wyalong and Condobolin Local Aboriginal Land Councils, and Wiradjuri Condobolin Corporation. They were then reburied at the original grave site.

## Radiocarbon dating

An attempt to extract collagen was made from two bones using an ultrafiltration protocol (Wood et al., 2014). The surface and as much material from the cracks as possible was removed with a dremel drill. Subsequently, the bones were crushed, demineralised in 0.5 M HCl overnight, treated with 0.1 M NaOH for 30 minutes and then 0.5 M HCl for 1 hour, gelatinised in pH3 at 70 $^{o}$C for 20 hours before Eeze$^{TM}$ filtration and ultrafiltration with a pre-cleaned Vivaspin$^{TM}$ VS15 30kDa MWCO ultrafilter. When the wt % collagen yield is less than 1 %, collagen is likely to be heavily altered and contaminants are difficult to remove (van Klinken, 1999).

## U-series

Three bone samples from the mandible (lab numbers 3008 to 3010) were analysed by laser ablation U-series at the Research School of Earth Sciences, Australian National University. Analyses were undertaken using a custom-built laser sampling system interfaced between an ArF excimer laser and a MC-ICP-MS Finnigan Neptune (for details see Eggins et al., 2003, 2005) following principles and procedures described in

Grün et al. (2014). Between 14 and 16 spots with diameters ~200 μm were analysed along four lines perpendicular to the outer bone surface (Fig. 3).

## Luminescence dating

Sample preparation for luminescence dating was designed to isolate pure extracts of 180-212 μm, quartz sand grains following standard procedures (e.g. Aitken, 1998). In a light-safe laboratory, treatments were applied to remove contaminant carbonates, feldspars, organics, heavy minerals and acid soluble fluorides. The outer ~10 μm alpha-irradiated rind of each grain was removed by etching in 40 % hydrofluoric acid for 40 min.

A burial dose was determined from measurement of the OSL signals emitted by single grains of quartz sand. The etched quartz grains were loaded on to custom-made, aluminium discs drilled with a 10 x 10 array of chambers, each 300 μm in depth and 300 μm in diameter (Bøtter -Jensen et al., 2000). The OSL measurements were made on a Risø TL/OSL DA-20 reader using a green (532 nm) laser for optical stimulation, and the ultraviolet emissions were detected by an Electron Tubes 9235QA photomultiplier tube fitted with 7.5 mm Hoya U-340 filter. Laboratory irradiations were conducted using a calibrated $^{90}Sr/^{90}Y$ beta source mounted on the reader. Equivalent doses ($D_e$) were determined using a modified SAR protocol (Olley et al., 2004). A dose-response curve was constructed for each grain. OSL signals were measured for 1 s at 125 °C (laser at 90 % power) using a preheat of 240 °C (held for 10 s) for the 'natural' and regenerative doses, and a pre-heat of 160 °C (held for 10 s) for the test doses (5 Gy). The OSL signal was determined from the initial 0.1 s of data, using the final 0.2 s to estimate the background count rate. Each disc was exposed to infrared (IR) radiation for 40 s at 125 °C prior to measurement of the OSL

signal to bleach any IR-sensitive signal. Dose recovery tests were undertaken to confirm that this treatment did not diminish the OSL signal from quartz and to check that the dose given in the laboratory could be successfully recovered under controlled conditions. Figure 4 provides the results of dose recovery tests undertaken using five different preheats, with preheats of 200 $^{o}$C or above providing measured /applied dose ratios of unity. Notably, all but the analyses done using a preheat of 160 $^{o}$C display zero overdispersion (or within uncertainty of zero in the case of 200 $^{o}$C preheat).

Grains were rejected if they did not produce a measurable OSL signal in response to the 5 Gy test dose, had OSL decay curves that did not reach background after 1 s of laser stimulation, produced natural OSL signals that did not intercept the regenerated dose-response curves, or had unacceptable sensitivity changes throughout the measurement cycle; i.e., they were rejected if either of the second or third Test Dose signals varied in sensitivity from the first Test Dose (associated with the Natural Dose) by more than 20 %. The proportion of accepted grains varied from 4 % (sample #9) to 12 % (samples #6 and #10). Failure to produce a measurable OSL signal in response to the test dose was responsible for the largest number of grain rejections, followed by unacceptable sensitivity changes through the measurement cycle. For the older samples (#7, #8, #9) the presence of saturated grains also resulted in additional grains being rejected, resulting in a lower accepted / analysed (a/n) ratio for these samples (see Table 3).

Lithogenic radionuclide activity concentrations of material extracted from sampling tubes were determined using high-resolution gamma spectrometry (Murray et al., 1987). Dose rates were calculated using the conversion factors of Stokes et al. (2003) with β-attenuation factors taken from Mejdahl (1979). Cosmic dose rates were

calculated from Prescott and Hutton (1994), with 0.4 m added to the measured depth for samples #1 to #9 to account for recent changes in burial depth due to erosion and vehicular compaction (see discussion). Long-term average water contents were estimated based on consideration of the measured water contents (see Table 2). Recent rain (at the time of sampling) likely elevated the water contents for the near-surface samples, hence the measured water contents for these samples are considered to be above the long-term average for these levee deposits which sit slightly above the surrounding plain. For these samples we have used a value of 10 ± 5 %. The samples at depth are considered more likely to be closer to their long-term average water content, hence a higher value (12.5 ± 5%), near the average of samples #7, #8, #9, has been selected. A very low water content of 2 % measured for sample #10 is attributed to post-sampling desiccation. Burial doses were calculated using age modelling techniques of Galbraith and co-workers (Galbraith and Green, 1990; Galbraith and Laslett, 1993; Galbraith et al., 1999; Roberts et al., 2000). First, the Central Age Model (CAM) was used to identify the level of over-dispersion ($\sigma_d$) within the single grain dose distributions. Over-dispersion is recognised as the spread in the data above that which would be expected from the measurement uncertainties on the individual single grain dose values. Contributors to $\sigma_d$ include partial bleaching, beta dose heterogeneity, bioturbation, differences between field and laboratory conditions and variable reliability of grains as dosimeters (Galbraith et al., 2005; Jacobs et al., 2006; Pietsch, 2009). Where $\sigma_d$ is low (<20 %) a burial dose was determined using the Central Age Model, on the assumption that most grains were fully bleached prior to burial and that small amounts of over-dispersion are to be expected based on the likely presence of some beta-dose heterogeneity and variation among individual $D_e$ uncertainty due to the likely sub-optimality of the analysis procedure for some grains.

The results of the dose recovery tests described above indicate that of these two, beta-dose heterogeneity is likely to be the dominant cause of the observed overdispersion, in line with previous research showing the prevalence and impact on dose distribution of beta dose heterogeneity (e.g. Jankowski and Jacobs, 2018). Where the $\sigma_d$ is high (>20 %) we have used the Finite Mixture Model (FMM) on the assumption that the principal contributor to $\sigma_d$ for our shallow buried samples will be bioturbation. Application of the FMM requires adding in quadrature to each single grain $D_e$ error the absolute percentage of $\sigma_d$ considered likely to have originated from sources other than partial bleaching or bioturbation: in other words, the $\sigma_d$ considered likely to have existed if no partial bleaching or bioturbation had occurred. To determine this value we have followed the approach of Pietsch et al. (2013), whereby the lowest $\sigma_d$ value observed from a suite of samples collected within a restricted geographical area (in this case 12 ± 1 % for sample 9) likely approximates the minimum possible $\sigma_d$ for that particular depositional environment. Hence this value should be used when applying the FMM. The number of samples analysed here is possibly too low for this method to be precise, so in part guided by the results from the larger sample sizes used elsewhere, we have selected 15 % as an appropriate added $\sigma_d$ (following Pietsch et al., 2013; and similar to Mueller et al., 2018). In addition to selecting an appropriate added $\sigma_d$ value, application of the FMM requires identifying the most appropriate number of dose components to use for each sample. We did this by observing the effect of changing the number of components on the Bayes Information Criterion, which attains its lowest value for the minimum number of parameters needed to explain the spread in data (Galbraith and Roberts, 2012). Table 3 provides the component number (*k*) used for each sample using this approach.

## Results

### Radiocarbon dating

Collagen yields from both bone samples were 0.1 % and they were not analysed further. This is not an uncommon situation in bones preserved in hot environments, and although it suggests that the bone is not very recent, it does not in itself indicate a Pleistocene antiquity (Collins et al., 2002).

### U-series

Uranium series results are shown in Table 1 and Figure 5. All isotopic ratios are expressed as activity ratios. Errors are reported at 2σ, including the calculated ages.

In general, U-series dates on bones have to be regarded as minimum age estimates. Modern bones and teeth are virtually U-free while fossils contain elevated U concentrations. Uranium is therefore taken up by the bone following burial. Two models have been proposed to account for U-uptake: the diffusion-adsorption (DA) model (e.g. Pike et al., 2002) and the diffusion-adsorption-decay (DAD) model of Sambridge et al. (2012). The former is based on closed system age calculations while the latter assumes a continuous U-diffusion. In young samples (<150 ka), the differences are minor (see Table 1). It should be noted that both open system models cannot recognise a longer period of little U-uptake followed by a more pronounced U-uptake, as often seems to be the case for open air sites.

Individual age results for each spot as well the relationships between the measured elemental U/Th ratios and ages are plotted in Figure 5. Because there is a relationship between measured $^{232}$Th and detrital $^{230}$Th leading to age overestimations, ages are usually only calculated where U/Th > 300. However, the samples show only a weak

relationship between $^{232}$Th and increased ages where U/Th < 30. Two of the largest outliers, spot 2 of 3008A and spot 5 of 3008B are associated with high U/Th values of > 600. None of the profiles show a depth-age relationship as expected from slow diffusion. Thus, we assume a fast diffusion process for which the best age estimation is derived from the mean values of the individual analyses. As can be seen from Table 1, there are small differences from the mean ages derived from all measurements and those that exclude Th/U< 30 and the two outliers. The best age estimate derives from the weighted mean of the tracks of 27.4 ± 0.4 ka (2σ error).

## Luminescence dating, sediments and radionuclide analysis

Augering adjacent to the Kiacatoo burial revealed 1.5 m of strong brown silty fine sand with rare carbonate nodules coarsening downwards to fine sand interpreted as a fluvial levee (Fig. 1D). This overlies 2.5 m of strong brown fine sandy silt and silty fine sand characteristic of lateral migration deposits with a weakly developed soil of brown, fine sandy, clayey silt evident in the uppermost 20 cm. The palaeomeander 220 m west of the burial was infilled to ~ 1 m of banktop with olive brown clayey silt and silty fine sand. Below 4.5 m was grey medium and coarse sand interpreted as channel bed sediments.

The measured radionuclide concentrations in samples collected for OSL dating are presented in Table 2. There is no evidence of significant disequilibria in the $^{238}$U decay series, the concentrations of $^{238}$U, $^{226}$Ra, and $^{210}$Pb being generally statistically indistinguishable at 2σ error. The exceptions to this are sample 1, which shows $^{210}$Pb loss, and samples 6 and 10, which show some excess $^{210}$Pb. The levels of disequilibria are unlikely to significantly affect the age calculations. The $^{40}$K activity concentrations show some variability between samples ranging from 342 ± 5 to 515 ±

9 Bq $kg^{-1}$, which probably results from variations in the clay/silt content. The calculated dose rates range from 1.7 ± 0.1 to 3.3 ± 0.3 Gy $ka^{-1}$.

All ten samples yielded quartz that proved suitable for single-grain OSL dating, but samples at shallow depths (<0.2 m) yielded different overdispersion characteristics to samples recovered from depths of 1 m and greater. Deeper samples had $D_e$ distributions with well-defined, single components, offering straightforward interpretation and burial dose calculations using the Central Age Model (Fig. 6, Table 3). In contrast, shallow samples associated with the grave infill and just below the grave boundary produced very mixed $D_e$ distributions. For these samples, the determination of depositional age was more problematic.

Samples collected at >1 m depth yielded ages of 29 ± 3 ka (#7) from the levee at 1 m depth, and 25 ± 2 (#8) from the lateral migration deposits at 2 m depth (Fig. 1D; Table 3). (Errors for all OSL ages are given at 1σ.) Underlying floodplain sediment at 4 m depth yielded an age of 42 ± 4 ka (#9). Bed sediment from the adjacent palaeochannel (LM1) yielded an age of 28 ± 2 ka at 4.6 m depth (#10, Fig. 1C). All of these samples yielded ages that are geomorphically and stratigraphically consistent when the uncertainties are taken into account.

Samples collected from < 0.3 m of the present surface yielded multi-modal dose distributions suggestive of significant post-depositional mixing. Table 3 provides ages calculated using each of the identified dose components. Ages for the grave infill based on the $D_e$ calculated using the largest component (i.e., the highest proportion), which in all but one case is also the youngest, range from 10 ± 1 ka (#5) to 17 ± 2 ka (#4). The same approach yields ages for samples immediately below the grave boundary of 16 ± 2 ka (#3) to 22 ± 2 ka (#2). These ages are equivalent within

uncertainties at 2σ. Sample #2 also has a proportionally minor (14 ± 4%) component centred on 36.2 ± 1.8 Gy that yields an age of 14 ± 1 ka, which may provide an indicative age for the overlying source material for intrusive grains. Notably, the degree of mixing as indicated by the $\sigma_d$ is broadly similar within the grave infill (21-35 %) and the sediment directly below (26-46 %). Examination of the secondary dose components, which have a proportional contribution of between 23 ± 6 % and 45 ± 16 % of grains, reveal a greater range in calculated ages for both the grave infill (17± 2 ka to 28 ± 4 ka) and the sediments immediately below (29 ± 3 ka to 43 ± 5 ka). It is worth noting that two samples (#2, #4) have ages calculated from the second component ($k_2$) that correspond with the U-series age of the skeleton at 27.4 ± 0.4 ka as well as with the OSL age on the levee, upper floodplain and channel bed sediments (25 ± 3 ka to 29 ± 3 ka). The $k_2$ component from a third sample (#1) overlaps with their age range at 2σ.

## Discussion

The use of a range of dating methods on the burial of Kiacatoo Man offers a relatively straightforward interpretation of the site chronology. U-series analysis provides a more direct age for the skeleton, but is regarded as a minimum age, as the uptake of uranium post-dates the burial itself. Interpretation of U-series ages on ancient human bones and teeth can be complicated by the open system behaviour of uranium, which is known to have influenced the apparent age in several cases and elsewhere on the Riverine Plains of southeast Australia (see review in Grün et al., 2014). This problem is, to some extent, resolved by the diffusion model applied to laser-ablated sub-samples across the sub-section of bone, and which suggests rapid U uptake (and no recent U loss) across all measured transects. However, the possibility of more complex uranium migration patterns cannot be excluded. It should be noted that open

system models cannot recognise a longer period of little U-uptake followed by a more pronounced U-uptake, as often seems to be the case for open air sites (Grün et al., 2010). In this case, the U-series age would underestimate the age of Kiacatoo Man by some unknown time.

Optically stimulated luminescence potentially can provide a precise age for human burial if it is applied to the infill sediment associated with the initial excavation and backfilling of the grave. This approach was used to date WLH3 ('Mungo Man') at 42±2 ka, independently verified by luminescence ages for sedimentary layers under and overlying the grave site (Bowler et al., 2003; Olley et al., 2006). This approach can be problematic where ongoing mixing (e.g. bioturbation) obscures the signals arising from grave opening and infill. More troubling still is the prospect that in some settings, the act of digging and infilling a grave can be insufficient to deplete the original depositional signal owing to the clustering of grave-dug sand grains (Kemp et al., 2014b). Luminescence ages for the sediment body into which a grave has been cut provide a maximum age only for the interred remains.

Here, the six near-surface OSL samples are characteristic of a complex exposure history rather than a discrete age that is clearly associated with a grave excavation event. Some samples have secondary $D_e$ concentrations (i.e. $k_2$ components – see Table 3) that broadly are consistent with those of the auger-hole samples. This might be related to a burial signal associated with grave cutting and filling that has been obscured by subsequent bioturbation or other disturbance. The critical question is whether the lower (i.e. the most recent) dose components evident in the grave infill samples relate to the burial event? If so, this would imply that the burial occurred ~11 ka, calculated as the average of $k_1$ ages from samples 5 and 6. Examination of the data

*in toto* suggests this is an unsound interpretation. If grave opening was responsible for the $k_1$ components then we would expect to see consistent calculated ages for the grave infill samples. Yet, the grave infill samples show a ~6 ka range in the $k_1$ ages. Furthermore, mixing, as represented by the percentage overdispersion (Table 3) is similar in both the grave-infill and in the underlying sediment (in fact slightly more in the sediment below the infill, see samples 1, 2 and 3); i.e. sediment that is unlikely to have been disturbed by grave excavation. This suggests that whatever process disturbed the grave infill was also responsible for disturbing the sediment beneath the grave, hence could not have been the cutting of the grave itself. From this we conclude that the $k_1$ ages obtained from the grave infill are the result of downward admixture of grains by bioturbation processes and other disturbances. Hence, they provide a minimum age for the burial.

Having identified post-depositional mixing as a likely agent affecting OSL dose distributions in the near-surface sediments, the absence of grains with a zero age, which would otherwise be taken as indicating that mixing was ongoing at the present day, requires some explanation. Their absence implies that OSL ages based on the youngest $D_e$ components, i.e. the ages based on the $k_1$ components (or the $k_3$ component in the case of sample #2) , likely represent the time since the sample was buried below the reach of disturbance processes such as bioturbation. This appears to have occurred below the grave at ~16 ka (average of $k_1$ ages for samples #1 and #3 and $k_3$ for sample #2) and, as expected, somewhat later for the shallower grave infill, of between ~17 ka (# 4) and ~11 ka (mean of #5 and #6). We surmise, based on the apparent absence of contemporary mixing, that there has been considerable erosion from the surface in recent decades, perhaps stripping 0.3 -0.6 m from the original height of the levee. This accords also with our expectation, based on cultural and

practical considerations, that the original grave would have been dug to ~0.6 m depth. Erosion on this scale has been reported elsewhere in the region owing to overgrazing by sheep and rabbits beginning in the 19th century with the effects still being felt in some semiarid areas (e.g. Fanning, 1994; Fitzsimmons et al., 2019). In the vicinity of the burial, erosion has been further enhanced by vehicular traffic.

The sediments and channels at the burial site provide relative evidence of the chronology of Kiacatoo Man, as well as his environmental context that will be examined in more detail in a subsequent paper. The floodplain and levee sedimentation at the burial site was occurring at ~27 ka (samples #7 and #8). Sandy sedimentation of the levee and channel probably continued until avulsion caused the relocation of the river to the contemporary Lachlan floodplain 1 km north. Geomorphological mapping suggests the cut-off meander dated at 28 ± 2 ka was constructed later than the channel and levee at the burial site. However, reliable OSL ages for the channel belt are similar or statistically identical at 1σ, and indicate that a channel larger than the present Lachlan existed during the period of extended cold that led up the Last Glacial Maximum in southeastern Australia (Petherick et al., 2013). During this interval, many of the lowland river systems of the Murray-Darling Basin experienced much larger discharges than at present (e.g. Hesse et al., 2018; Mueller et al., 2018). The previously undated channel belt at Kiacatoo loses distinctness upstream, where it is cut by the modern Lachlan floodplain. Downstream, it merges with large wavelength meanders and scroll plain characteristic of the Ulgutherie Palaeochannel System (Kemp and Spooner, 2007; Kemp and Rhodes, 2010), which here have been partly reworked by a river of smaller dimensions and by the modern Borapine Creek. Fluvial sediments with an age of 42 ± 4 ka (#9) recovered from deeper in the floodplain might have formed part of the Ulgutherie

system. The geomorphic and stratigraphic associations between the palaeochannel and the modern and Ulgutherie systems allow us to coarsely bracket the palaeochannel-levee age as between about 20 and 34 ka (i.e. the age of the Ulgutherie system) and the development of the smaller, modern channel belt before ~8 ka (Kemp and Rhodes, 2010; Kemp et al., 2017). The time of abandonment of the channel belt that hosts Kiacatoo Man could not be established, but channel bed sediments were subsequently buried by <5 m of fine-textured sediment deposited during floods from the Lachlan and Borapine Creek and which continues in the present day. Disturbance of the upper levee sediments (by, for example, bioturbation) continued until ~10 ka when the grave location appears to have been below the reach of disturbance. Erosion, of at least 0.4 m, much of it possibly during the last 200 years, then exposed the upper boundary of the Kiacatoo skeleton.

## Conclusion

The results from radiocarbon, uranium series, and luminescence dating together with the sedimentary and geomorphic analysis provide a range of direct and indirect methods to establish the age of the ancient human remains of Kiacatoo Man in semiarid riverine plains in southeastern Australia. Well-defined single component, single grain OSL distributions on undisturbed floodplain sediments underlying the grave provide a maximum age for the burial of 26.4± 1.5 ka (the weighted mean age of samples #7 and #8). OSL ages on sediment within and immediately beneath the grave reflect the effects of post-depositional mixing (such as bioturbation and anthropogenic disturbance) over a period extending from ~27 ka to ~10 ka. The OSL age for the underlying, undisturbed sediment is supported by U-series analysis on bone, which provides a minimum age for the skeleton itself of 27.4 ± 0.4 ka. The close bracketing of minimum and maximum ages implies a burial age for the skeleton,

at the 95 % confidence interval, of older than 27.0 ka (the lower 2σ limit of the U-series age) and younger than 29.4 ka (the upper 2σ limit of the OSL age). These results emphasise the value of a multi-method approach in dating ancient human fossils in the semiarid and hot environments typical of inland Australia.

Acknowledgments

We would like to thank Phil Purcell, NSW Office of Environment and Heritage, for organising the excavation and reburial of Kiacatoo Man, Ron and the late George Cocos for access to their property, 'Cocos'. The Wiradjuri traditional owners authorised excavation of the remains and further analysis including dating. We thank the supporting Wiradjuri organisations that participated: Wiradjuri Condobolin Corporation, and Murrin Bridge, Condobolin and West Wyalong Local Aboriginal Land Councils. We were assisted in the field by Nicole Pietsch and by enthusiastic Wiradjuri volunteers from Lake Cargelligo, Condobolin, and by members of the Lake Cargelligo Local Historical Society, particularly Mr and Mrs Steve Johnson, Leeanne Hampton and Linton Howards of West Wyalong. The Local Aboriginal Land Councils have continued to support our efforts during and since the excavation. The manuscript was greatly improved by helpful comments by Richard (Bert) Roberts and Matthew Cupper. This research was funded by the Australian Research Council [grant no LP130100748].

References

Aitken, M.J., 1998. An Introduction to Optical Dating: The Dating of Quaternary Sediments by the Use of Photon-stimulated Luminescence. Oxford University Press, Oxford.

Bøtter-Jensen, L., Bulur, E., Duller, G.A.T., Murray, A.S., 2000. Advances in luminescence instrument systems. Radiation Measurements 32, 523-528.

Bowler, J.M., 1998., Willandra Lakes revisited: environmental framework for human occupation. Archaeology in Oceania 33, 120-155.

Bowler, J.M., Magee, J.W., 2000. Redating Australia's oldest humans remains: a sceptic's view. Journal of Human Evolution 38, 719-726.

Bowler, J.M., Johnston, H., Olley, J.M., Prescott, J.R., Roberts, R.G., Shawcross, W., Spooner, N.A., 2003. New ages for human occupation and climate change at Lake Mungo, Australia. Nature 421, 837-840.

Collins, M.J., Nielsen-Marsh, C.M., Hiller, J., Smith, C.I., Roberts, J.P., Prigodich, R.V., Wess, T.J., Csapò, J., Millard, A.R., Turner-Walker, G., 2002. The survival of organic matter in bone: a review. Archaeometry 44, 383-394.

Eggins, S., Grün, R., Pike, A., Shelley, A., Taylor, L., 2003. $^{238}U$, $^{232}Th$ profiling and U-series isotope analysis of fossil teeth by laser ablation ICPMS. Quaternary Science Reviews 22, 1373-1382.

Eggins, S.M., Grün, R., McCulloch, M.T., Pike, A.W.G., Chappell, J., Kinsley, L., Shelley, M., Murray-Wallace, C.V., Spötl, C., Taylor, L., 2005. In situ U-series dating by laser ablation multi-collector ICPMS: new prospects for Quaternary geochronology. Quaternary Science Reviews 24, 2523-2538.

Fanning, P., 1994. Long-term contemporary erosion rates in an arid rangelands environment in western New South Wales, Australia. Journal of Arid Environments 28, 173-187.

Fitzsimmons, K.E., Stern, N., Murray-Wallace, C.V., 2014. Depositional history and archaeology of the central Lake Mungo lunette, Willandra lakes, southeast Australia. Journal of Archaeological Science 41, 349-364.

Fitzsimmons, K.E., Stern, N., Murray-Wallace, C.V., Truscott, W., Pop, C., 2015. The Mungo mega-lake event, semi-arid Australia: non-linear descent into the last ice age, implications for human behaviour. PLoS ONE 10(6), e0127008.

Fitzsimmons, K.E., Spry, C., Stern, N., 2019. Holocene and recent aeolian reactivation of the Willandra Lakes lunettes, semi-arid southeastern Australia. The Holocene 29, 606-621.

Galbraith, R.F., Green, P.F., 1990. Estimating the component ages in a finite mixture. International Journal of Radiation Applications and Instrumentation. Part D. Nuclear Tracks and Radiation Measurements 17, 197-206.

Galbraith, R.F., Laslett, G.M., 1993. Statistical models for mixed fission track ages. Nuclear Tracks and Radiation Measurements 21, 459-470.

Galbraith, R.F., Roberts, R.G., Laslett, G.M., Yoshida, H., Olley, J.M., 1999. Optical dating of single and multiple grains of quartz from Jimnium rock shelter, northern Australia: Part I. Experimental design and statistical models. Archaeometry 41, 339-364.

Gillespie, R., Roberts, R.G., 2000. On the reliability of age estimates for human remains at Lake Mungo. Journal of Human Evolution 38, 727–732.

Galbraith, R.F., Roberts, R.G., Yoshida, H., 2005. Error variation in OSL palaeodose estimates from single aliquots of quartz. Radiation Measurements. 39. 289-307.

Grün, R., Spooner, N.A., Thorne, A., Mortimer, G., Simpson, J.J., McCulloch, M.T., Taylor, L., Curnoe, D., 2000. Age of the Lake Mungo 3 skeleton, reply to Bowler & Magee and to Gillespie & Roberts. Journal of Human Evolution 38, 733-741.

Grün, R., Aubert, M., Hellstrom, J., Duval, M., 2010. The challenge of direct dating old human fossils. Quaternary International 223, 87-93.

Grün, R., Eggins, S., Kinsley, L., Mosely, H., Sambridge, M., 2014. Laser ablation U-series analysis of fossil bones and teeth. Palaeogeography, Palaeoclimatology, Palaeoecology 416, 150-167.

Gillespie, R., 1998. Alternative timescales: a critical review of Willandra Lakes dating. Archaeology in Oceania 33, 169–182.

Hesse, P.P., Williams, R., Ralph, T.J., Fryirs, K.A., Larkin, Z.T., Westaway, K.E., Farebrother, W., 2018. Palaeohydrology of lowland rivers in the Murray-Darling Basin, Australia. Quaternary Science Reviews 200, 85-105.

Hill, E.C., Durband, A.C., 2014. Mobility and subsistence at the Willandra lakes: a comparative analysis of femoral cross-sectional properties in the Lake Mungo 3 skeleton. Journal of Human Evolution 73, 103-106.

Jacobs, Z., Duller, G.A.T., Wintle, A.G., 2006. Interpretation of single grain $D_e$ distributions and calculation of $D_e$. Radiation Measurements 41, 264–277.

Jankowski, N.R., Jacobs, Z., 2018. Beta dose variability and its spatial contextualisation in samples used for optical dating: An empirical approach to examining beta microdosimetry. Quaternary Geochronology 44, 23-37.

Kemp, J., Spooner, N.A., 2007. Evidence for regionally wet conditions before the LGM in southeast Australia: OSL ages from a large palaeochannel in the Lachlan Valley. Journal of Quaternary Science 22, 423-427.

Kemp, J., Rhodes, E.J., 2010. Episodic fluvial activity of inland rivers in southeastern Australia: palaeochannel systems and terraces of the Lachlan River. Quaternary Science Reviews 29, 732-752.

Kemp, J., Gontz, A., Pardoe, C., Pietsch, T., Olley, J., 2014a. A ground-penetrating radar survey near the excavated burial site of Kiacatoo Man. Quaternary Australasia 31, 32-39.

Kemp, J., Pietsch, T.J., Olley, J.M., 2014b. Digging your own grave: OSL signatures in experimental graves. Journal of Human Evolution 76, 77-82.

Kemp, J., Pietsch, T., Gontz, A., Olley, J., 2017. Lacustrine-fluvial interactions in Australia's Riverine Plains. Quaternary Science Reviews 166, 352-362.

Long, K., Stern, N., Williams, I.S., Kinsley, L., Wood, R., Sporcic, Smith, T., Fallon, S., Kokkenen, H., Moffat, I., Grün, R., 2014. Fish otolith geochemistry, environmental conditions and human occupation at Lake Mungo, Australia. Quaternary Science Reviews 88, 82-95.

Mejdahl, V., 1979. Thermoluminescence dating: beta-dose attenuation in quartz grains. Archaeometry 21, 61-72.

Mueller, D., Jacobs, Z., Cohen, T.J., Price, D.M., Reinfelds, I.V., Shulmeister, J., 2018. Revisiting an arid LGM using fluvial archives: a luminescence chronology

for palaeochannels of the Murrumbidgee River, south-eastern Australia. Journal of Quaternary Science 33, 777-793.

Murray, A.S., Marten, R., Johnston, A., Martin, P., 1987. Analysis for naturally occurring radionuclides at environmental concentrations by gamma spectrometry. Journal of Radioanalytical and Nuclear Chemistry 115, 263-288.

Olley, J.M., Pietsch, T., Roberts, R.G., 2004. Optical dating of Holocene sediments from a variety of geomorphic setting using single grains of quartz. Geomorphology 60, 337-358.

Olley, J.M., Roberts, R.G., Yoshida, H., Bowler, J.M., 2006. Single-grain optical dating of grave-infill associated with human burials at Lake Mungo, Australia. Quaternary Science Reviews 25, 2469-2474.

Pardoe, C., 1990. The demographic basis of human evolution in southeastern Australia. In: Meehan, B., White, N. (Eds.), Hunter-gatherer Demography. Oceania Monograph 9. University of Sydney Press, Sydney, pp. 59-70.

Pardoe, C. 1993. The Pleistocene is still with us. Analytical constraints and possibilities for the study of ancient human remains in archaeology. In: Smith, M.A., Spriggs, M., Fankhauser, B. (Eds.) Sahul in Review: Pleistocene archaeology in Australia, New Guinea and Island Melanesia. Occasional Papers from the Department of Prehistory, Research School of Pacific Studies, Australian National University, Canberra, pp. 81-94.

Pardoe, C., 1995. Riverine, biological and cultural evolution in southeastern Australia. Antiquity 69, 696-713.

Pardoe, C., 2006. Becoming Australian: evolutionary processes and biological variation from ancient to modern times. Before Farming [online version] 2006/1 article 4, 1-21.

Pardoe, C., 2010. Global human variation: polarised positions and alternative perspectives. Before Farming [online version] 2010/3 article 3, 1-21.

Petherick, L., Bostock, H., Cohen, T.J., Fitzsimmons, K., Tibby, J., Fletcher, M.S., Moss, P., Reeves, J., Mooney, S., Barrows, T., Kemp, J., Jansen, J., Nanson, G., Dosseto, A., 2013. Climatic records over the past 30 ka from temperate Australia–a synthesis from the Oz-INTIMATE workgroup. Quaternary Science Reviews 74, 58-77.

Pietsch, T.J., 2009. Optically stimulated luminescence dating of young (b500 years old) sediments: testing estimates of burial dose. Quaternary Geochronology 4, 406–422.

Pietsch, T.J., Nanson, G.C., Olley, J.M., 2013. Late Quaternary changes in flow-regime on the Gwydir distributive fluvial system, southeastern Australia. Quaternary Science Reviews 69, 168-180.

Pike, A.W.G., Hedges, R.E.M., van Calsteren, P., 2002. U-series dating of bone using the diffusion-adsorption model. Geochimica et Cosmochimica Acta 66, 4273-4286.

Prescott, J.R., Hutton, J.T., 1994. Cosmic ray contributions to dose rates for luminescence and ESR dating: large depths and long term time variations. Radiation Measurements 23, 497-500.

Roberts, R.G., Galbraith, R.F., Yoshida, H., Laslett, G.M., Olley, J.M., 2000. Distinguishing dose populations in sediment mixtures: a test of single-grain optical dating procedures using mixtures of laboratory-dosed quartz. Radiation Measurements 32, 459-465.

Sambridge, M., Grün, R., Eggins, S., 2012. U-series dating of bone in an open system: the diffusion-adsorption-decay model. Quaternary Geochronology 9, 42-53.

Stern, N., Tumney, J., Fitzsimmons, K.E., Kajewski, P., 2013. Strategies for investigating human responses to changes in landscape and climate at Lake Mungo in the Willandra Lakes, southeast Australia. In: Frankel, D., Webb, J., Lawrence, S. (Eds.), Archaeology in Environment and Technology: Intersections and Transformations. Routledge, New York, pp. 31-50.

Stern, N., 2015. The archaeology of the Willandra. In: McGrath, A., Webb, M.A. (Eds.), Long History, Deep Time: Deepening Histories of Place. ANU Press & Aboriginal History, Canberra, pp. 221-240.

Stokes, S., Ingram, S., Aitken, M.J., Sirocko, F., Anderson, R., Leuschner, D., 2003. Alternative chronologies for Late Quaternary (Last Interglacial-Holocene) deep sea sediment via optical dating of silt-size quartz. Quaternary Science Reviews 22, 925-941.

Thorne A., Grün, R., Mortimer, G., Spooner, N.A., Simpson, J.J., McCulloch, M., Taylor, L., Curnoe, D., 1999. Australia's oldest human remains: age of the Lake Mungo 3 skeleton. Journal of Human Evolution 36, 591–612.

van Klinken, G.J., 1999. Bone collagen quality indicators for palaeodietary and radiocarbon measurements. Journal of Archaeological Science 26, 687-695.

Wood, R.E., Arrizabalaga Valbuena, A., Camps, M., Fallon, S., Iriarte-Chiapusso, M.J., Jones, R., Maroto, J., de la Rasilla, M., Santamaría, D., Soler, J., Soler, N., Villaluenga, A., Higham, T.F.G., 2014. The chronology of the earliest Upper Palaeolithic in northern Iberia: new insights from L'Arbreda, Labeko Koba and La Viña. Journal of Human Evolution 69, 91-109.

## Figures

Figure 1. A. Location of Kiacatoo within the riverine plains of the Murray Basin in southeastern Australia. B. Grave excavation cross-section. Six OSL samples (circled) were collected from within or immediately below the weakly defined grave boundary. C. Geomorphic map of the Lachlan River and floodplain at Kiacatoo, showing the burial location, core CL12 through the levee, and the palaeomeander sampled at a depth of 4.6 m from bedload sediment (LM1, sample #10). Corresponding OSL ages are given in ka. D. Borehole sediment log for CL12. Three samples were collected at depths of 1, 2 and 4 m within the levee. Numbered circles indicate the location of OSL samples, and ages are shown in ka. Table 3 provides laboratory codes for each sample.

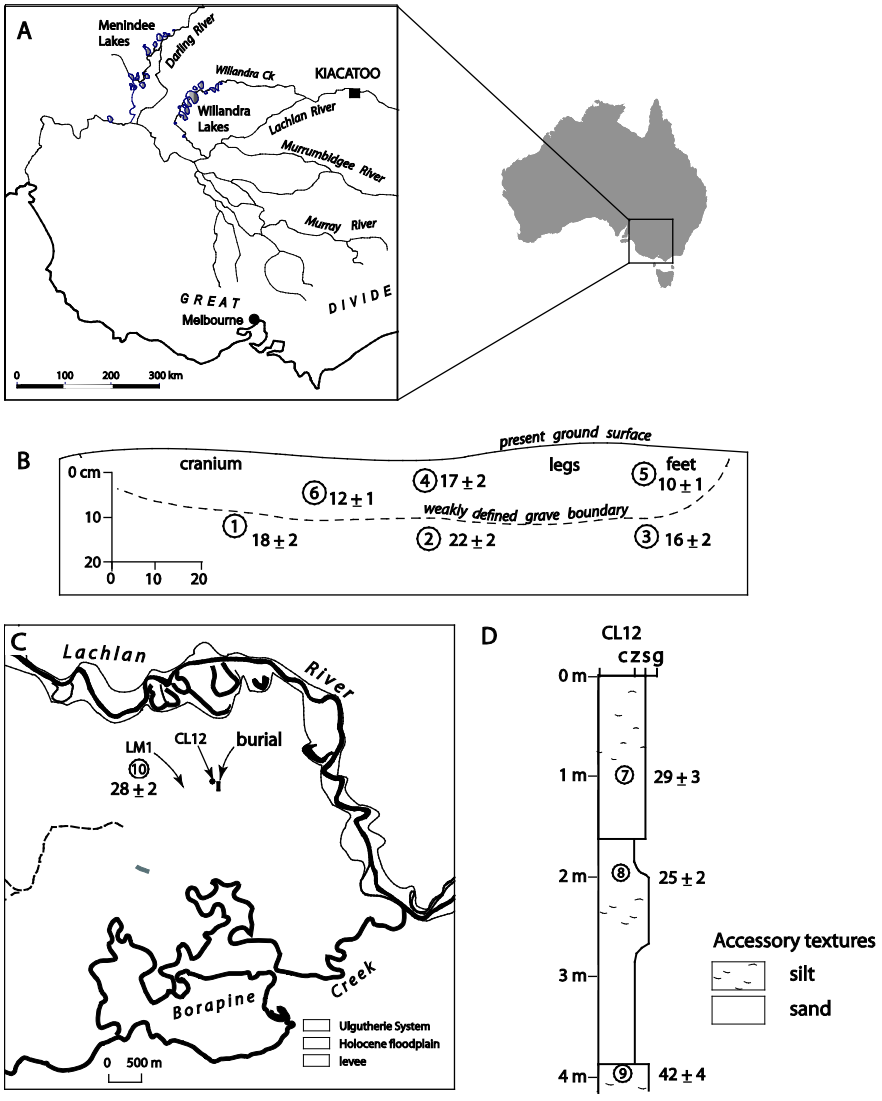

Figure 2: A. Exposed side of burial site, showing the locations of OSL samples #1 - #5. Fragments of the cranium are visible after preliminary excavation of the ground surface. B. Post-cranial skeleton of Kiacatoo Man during excavation. OSL sample #6 was extracted vertically behind the thorax.

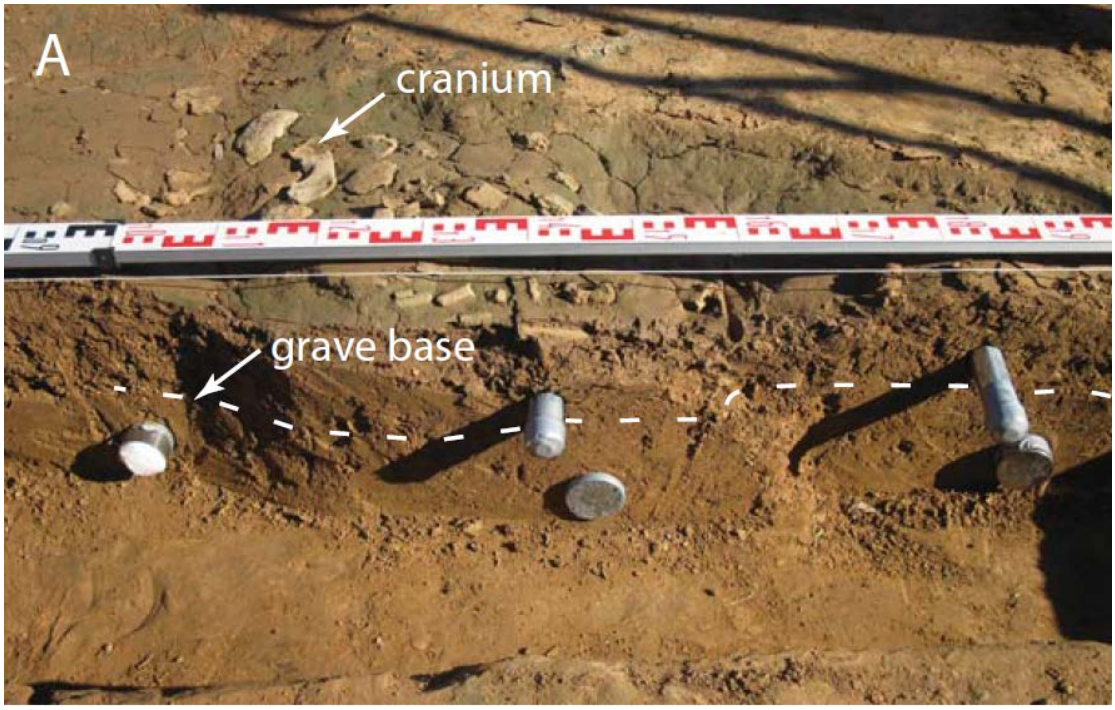


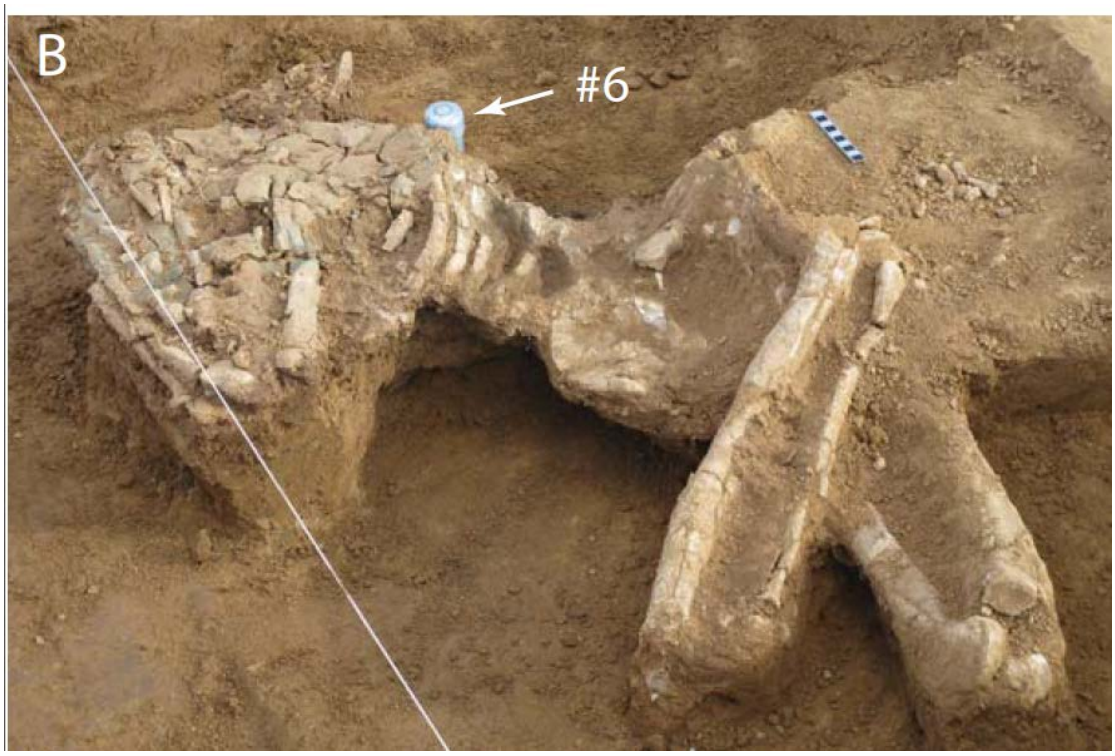

Figure 3**:** Bone samples showing sampling locations (using laser-ablation) for U-series analysis.

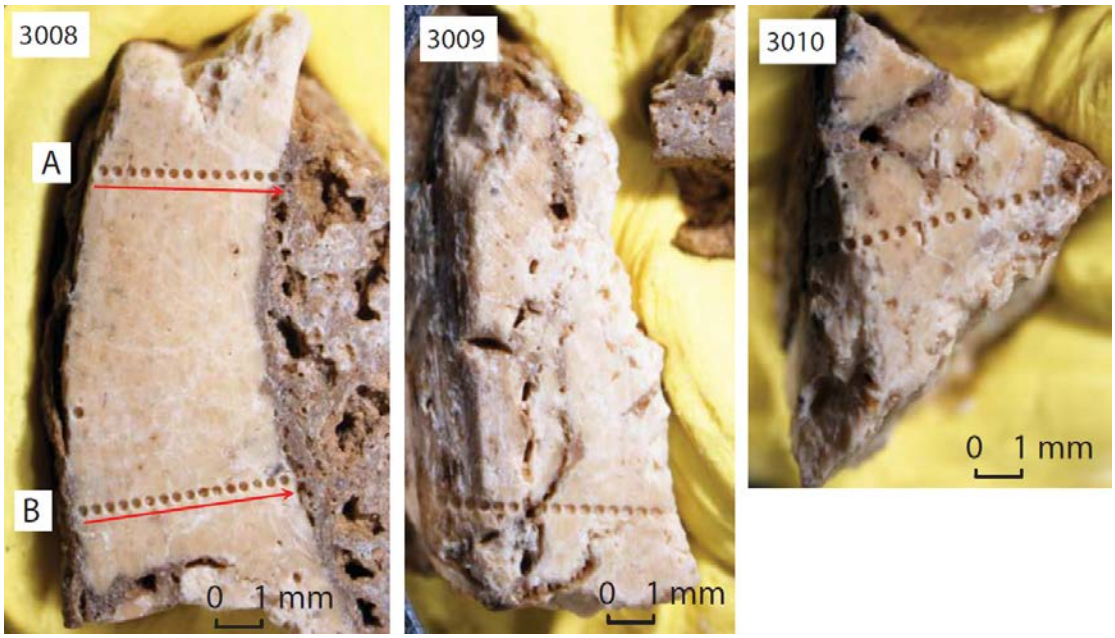

Figure 4: Results of dose recovery tests, whereby a sample (#9) is bleached of its natural dose then provided with a laboratory applied dose (~41.5 Gy). The sample is then subject to the standard analysis protocol in an attempt to recover the known dose. In this case we have undertaken the dose recovery tests at multiple preheat temperatures, ranging from 160 °C to 240 °C. Five of the panes provide radial plots of dose distributions produced from analysis of the five samples provided with the known dose. The measured $D_e$ (in Gy) for a grain can be read by tracing a line from the y-axis origin through the point until the line intersects the radial axis (log scale) on the right-hand side. The corresponding standard error for this estimate can be read by extending a line vertically to intersect the x-axis. The x-axis has two scales: one plots the relative standard error of the $D_e$ estimate (in %) and the other ('Precision') plots the reciprocal standard error. Therefore, values with the highest precisions and the smallest relative errors plot closest to the radial axis on the right of the diagram, and the least precise estimates plot furthest to the left. Values within the grey shaded bands are within 2 σ of the recovered dose, as determined using the Central Age Model. The solid line corresponds with the applied dose of ~41.5 Gy. Each of the radial plots is also annotated with the measured overdispersion ($\sigma_d$). The sixth pane plots the ratio of the measured dose (determined using the CAM) to the applied dose for each of the preheat temperatures. The dashed line indicates unity.

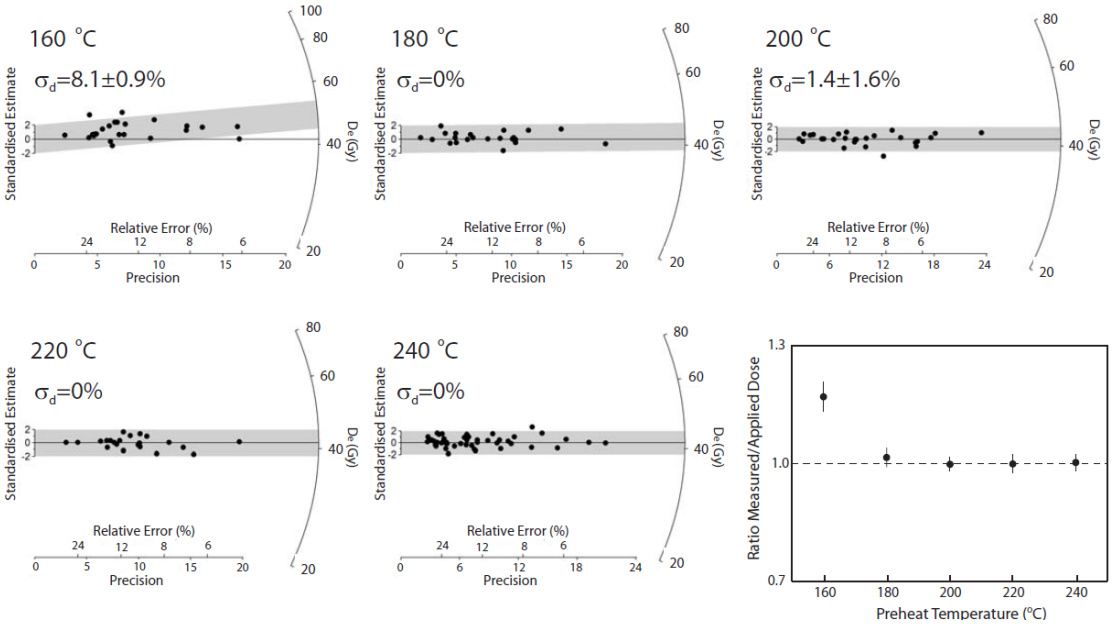

Figure 5: Results of U-series analysis showing calculated age for each spot (left column) and the same data plotted against U/Th ratio. The solid line indicates the weighted mean averages as provided in Table 1 with dashed lines indicating 1σ errors.

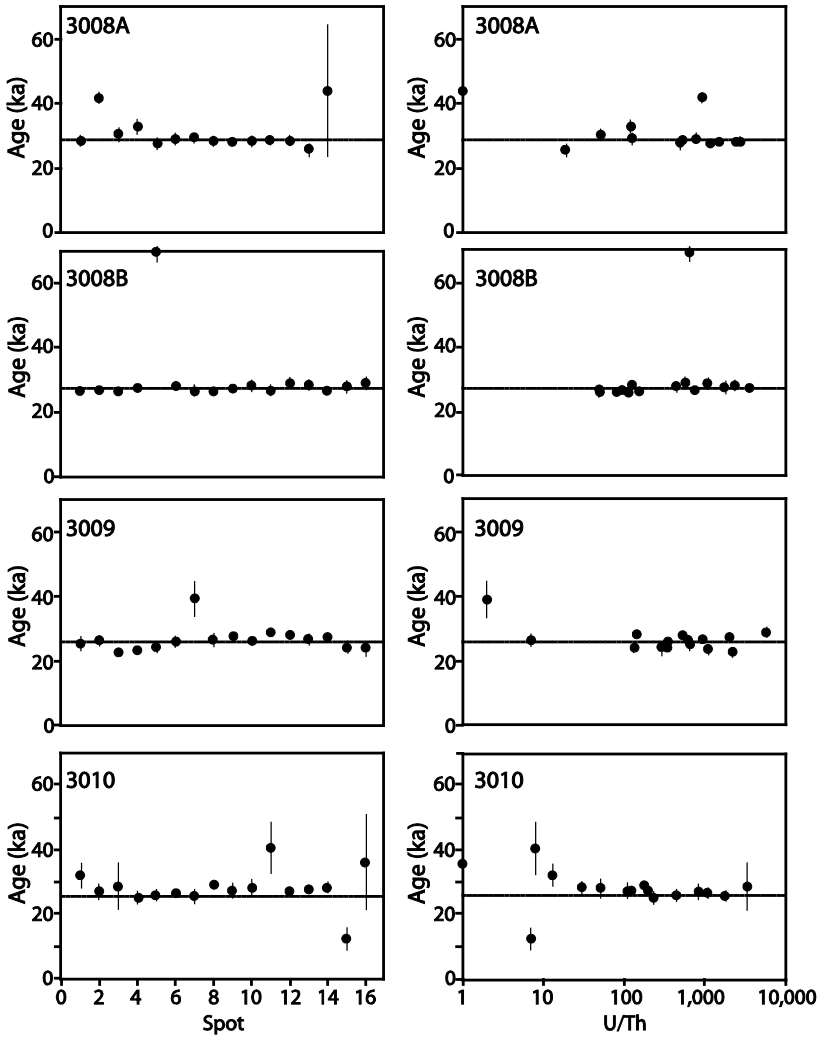

Figure 6: Radial plots for all samples. Values within the grey shaded bands are within 2 σ of the dose components calculated using the Finite Mixture Model (Galbraith and Green, 1990; Galbraith and Laslett, 1993; Galbraith et al., 1999; Roberts et al., 2000) with an applied overdispersion parameter of 15 %. For samples fitted with two components, the component making up the largest proportion of grains ($k_1$) is shown in light grey, with the minor component ($k_2$) shown in dark grey. For clarity, only the two dose components having the highest proportions are highlighted for sample #2.

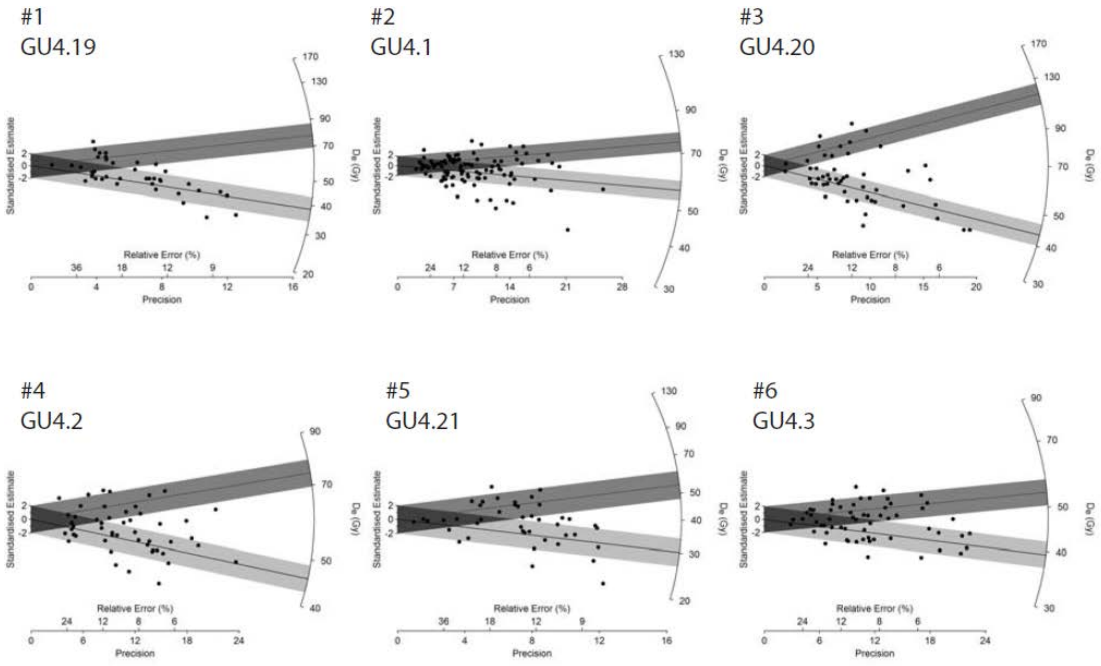

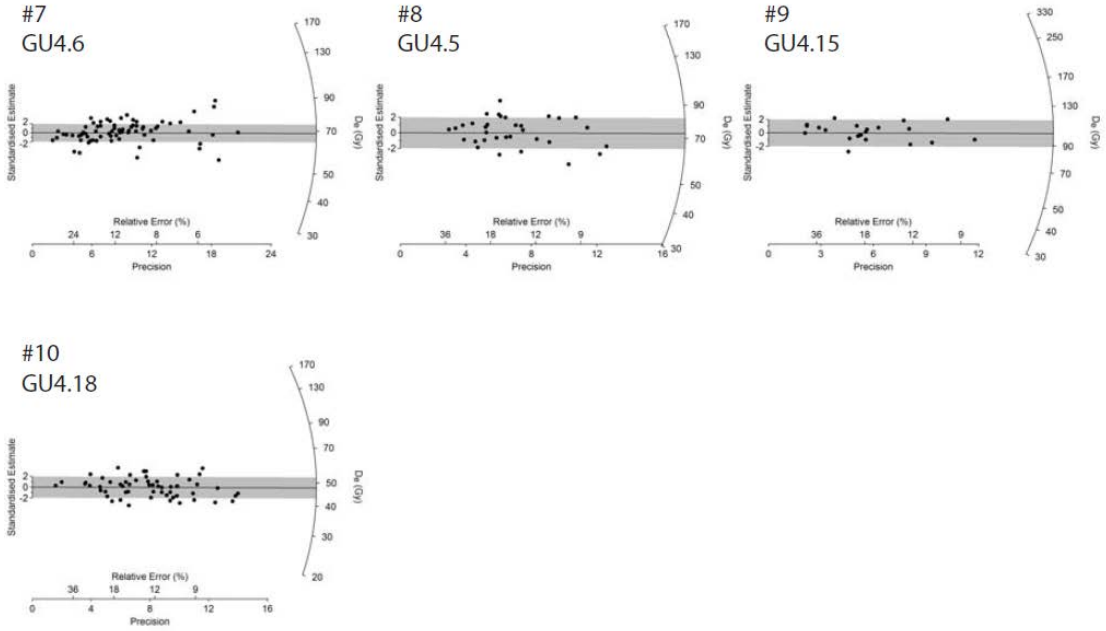


**Table 1:** U-series results on human bone from Kiacatoo. All errors are 2σ. Individual results do not contain errors of standard measurement (correlated errors), mean values incorporate errors of standard. CS calculations are based on closed system assumptions while diffusion (Diff) ages are based on the continuous diffusion assumption of Sambridge et al. (2012).

| 3008A | U (ppm) | Th (ppb) | U/Th | $^{230}Th/^{238}U$ | $^{234}U/^{238}U$ | CS Age (ka) | Diff Age (ka) |
|---|---|---|---|---|---|---|---|
| 1 | 24.08 | 15 | 1559 | 0.3222±0.0117 | 1.3913±0.01 | 28.4±1.2 | 28.8±1.2 |
| 2 | 22.99 | 25 | 904 | 0.4486±0.0117 | 1.3917±0.0107 | 41.7±1.4 | 42.5±1.3 |
| 3 | 12.96 | 256 | 51 | 0.3427±0.0159 | 1.3971±0.0113 | 30.3±1.6 | 30.7±1.6 |
| 4 | 16.65 | 140 | 119 | 0.3681±0.0211 | 1.4088±0.015 | 32.6±2.2 | 33.1±2.2 |
| 5 | 20.58 | 42 | 490 | 0.3143±0.0155 | 1.3907±0.012 | 27.6±1.6 | 28±1.6 |
| 6 | 17.22 | 139 | 124 | 0.3256±0.0155 | 1.3823±0.012 | 29±1.6 | 29.3±1.6 |
| 7 | 18.12 | 23 | 780 | 0.3301±0.0117 | 1.3931±0.0122 | 29.2±1.2 | 29.5±1.2 |
| 8 | 19.47 | 8 | 2441 | 0.3203±0.0102 | 1.3929±0.0134 | 28.2±1.1 | 28.5±1 |
| 9 | 17.64 | 15 | 1192 | 0.3195±0.0107 | 1.4027±0.0163 | 27.9±1.1 | 28.2±1.1 |
| 10 | 17.86 | 34 | 518 | 0.32±0.0095 | 1.3891±0.0152 | 28.2±1 | 28.6±1 |

| | | | | | | | |
|---|---|---|---|---|---|---|---|
| 11 | 15.48 | 10 | 1490 | 0.3222±0.013 | 1.3881±0.0135 | 28.5±1.3 | 28.8±1.3 |
| 12 | 16.44 | 6 | 2698 | 0.3226±0.0099 | 1.3952±0.0134 | 28.4±1 | 28.7±1 |
| 13 | 10.84 | 566 | 19 | 0.2967±0.0172 | 1.4032±0.0322 | 25.6±1.8 | 25.9±1.7 |
| 14 | 3.29 | 2252 | 1 | 0.4479±0.1686 | 1.3335±0.1 | 43.9±20.4 | 44.7±20.8 |
| **Mean Values** | | | | | | | |
| 1-14 | 16.69±2.78 | | | 0.3393±0.0068 | 1.3929±0.0084 | 30.1±0.7 | 30.5±0.7 |
| ex 2, 13, 14 | 17.86±1.71 | | | 0.3271±0.0066 | 1.3935±0.0084 | 28.8±0.7 | 29.2±0.7 |

| 3008 B | U (ppm) | Th (ppb) | U/Th | $^{230}Th/^{238}U$ | $^{234}U/^{238}U$ | CS Age (ka) | Diff Age (ka) |
|---|---|---|---|---|---|---|---|
| 1 | 22.43 | 31 | 734 | 0.3027±0.0102 | 1.3859±0.0088 | 26.6±1 | 26.9±1 |
| 2 | 21.88 | 141 | 155 | 0.3033±0.0116 | 1.3912±0.0116 | 26.5±1.2 | 26.8±1.2 |
| 3 | 22.1 | 258 | 86 | 0.3035±0.0122 | 1.3941±0.014 | 26.5±1.2 | 26.8±1.2 |
| 4 | 21.12 | 6 | 3603 | 0.3099±0.0137 | 1.3891±0.0104 | 27.2±1.4 | 27.6±1.4 |
| 5 | 20.11 | 31 | 649 | 0.6738±0.0202 | 1.3927±0.0114 | 69.6±2.9 | 72.2±3.1 |
| 6 | 16.6 | 37 | 445 | 0.3175±0.0106 | 1.3947±0.0196 | 27.9±1.1 | 28.2±1.1 |
| 7 | 17.6 | 112 | 157 | 0.3039±0.0137 | 1.3923±0.0136 | 26.6±1.4 | 26.9±1.4 |
| 8 | 17.02 | 152 | 112 | 0.3043±0.015 | 1.3986±0.012 | 26.5±1.5 | 26.8±1.5 |
| 9 | 15.16 | 158 | 96 | 0.3092±0.0129 | 1.3929±0.0142 | 27.1±1.3 | 27.4±1.3 |

| | | | | | | | |
|---|---|---|---|---|---|---|---|
| 10 | 16.18 | 130 | 124 | 0.3227±0.0139 | 1.3997±0.0141 | 28.3±1.4 | 28.6±1.4 |
| 11 | 11.43 | 230 | 50 | 0.3064±0.0131 | 1.3963±0.0179 | 26.7±1.3 | 27.1±1.3 |
| 12 | 17.47 | 31 | 566 | 0.3277±0.0171 | 1.3909±0.0206 | 29±1.8 | 29.3±1.8 |
| 13 | 14.93 | 6 | 2341 | 0.3229±0.0133 | 1.3998±0.0132 | 28.3±1.3 | 28.6±1.3 |
| 14 | 10.85 | 223 | 49 | 0.2988±0.0128 | 1.3857±0.0184 | 26.2±1.3 | 26.5±1.3 |
| 15 | 14.59 | 8 | 1782 | 0.3157±0.0192 | 1.3936±0.0159 | 27.7±1.9 | 28±1.9 |
| 16 | 16.4 | 15 | 1096 | 0.3312±0.0102 | 1.4012±0.0135 | 29.1±1.1 | 29.5±1 |
| **Mean Values** | | | | | | | |
| 1-16 | 17.24±1.78 | | | 0.3381±0.0065 | 1.3935±0.0082 | 29.9±0.7 | 30.3±0.7 |
| ex 5 | 17.05±1.85 | | | 0.3117±0.0061 | 1.3935±0.0082 | 27.3±0.6 | 27.6±0.6 |

| 3009 | U (ppm) | Th (ppb) | U/Th | $^{230}Th/^{238}U$ | $^{234}U/^{238}U$ | CS Age (ka) | Diff Age (ka) |
|---|---|---|---|---|---|---|---|
| 1 | 23.94 | 38 | 631 | 0.2926±0.0201 | 1.3934±0.0171 | 25.5±2 | 25.7±2 |
| 2 | 24.8 | 40 | 614 | 0.3006±0.01 | 1.387±0.013 | 26.4±1 | 26.7±1 |
| 3 | 18.15 | 8 | 2170 | 0.2672±0.0107 | 1.3969±0.0116 | 22.9±1 | 23.2±1 |
| 4 | 20.24 | 19 | 1085 | 0.2726±0.0114 | 1.3841±0.0121 | 23.7±1.1 | 24±1.1 |
| 5 | 14.11 | 42 | 338 | 0.2793±0.0146 | 1.3812±0.0154 | 24.4±1.4 | 24.7±1.4 |
| 6 | 16.75 | 49 | 341 | 0.2971±0.0134 | 1.3813±0.0128 | 26.1±1.4 | 26.4±1.4 |
| 7 | 4.45 | 1941 | 2 | 0.4112±0.0483 | 1.3412±0.0204 | 39.3±5.5 | 40±5.7 |

| | | | | | | | |
|---|---|---|---|---|---|---|---|
| 8 | 9.5 | 1307 | 7 | 0.3013±0.0184 | 1.3818±0.0217 | 26.6±1.9 | 26.9±1.9 |
| 9 | 20.01 | 37 | 534 | 0.314±0.0099 | 1.379±0.0129 | 27.9±1 | 28.2±1 |
| 10 | 20.49 | 21 | 953 | 0.2985±0.0081 | 1.381±0.0109 | 26.3±0.8 | 26.6±0.8 |
| 11 | 22.04 | 4 | 5699 | 0.3289±0.0091 | 1.3943±0.0093 | 29±0.9 | 29.4±0.9 |
| 12 | 16.44 | 111 | 147 | 0.3198±0.0105 | 1.3864±0.0138 | 28.3±1.1 | 28.6±1.1 |
| 13 | 22.26 | 24 | 941 | 0.3042±0.0108 | 1.3853±0.0103 | 26.8±1.1 | 27.1±1.1 |
| 14 | 23.87 | 12 | 2021 | 0.31±0.0086 | 1.3883±0.0116 | 27.3±0.9 | 27.6±0.9 |
| 15 | 16.78 | 128 | 132 | 0.2824±0.0152 | 1.3951±0.0152 | 24.4±1.5 | 24.7±1.5 |
| 16 | 18.13 | 62 | 292 | 0.2786±0.0236 | 1.3939±0.0212 | 24.1±2.3 | 24.4±2.3 |
| **Mean Values** | | | | | | | |
| 1-16 | 18.25±2.71 | | | 0.299±0.0059 | 1.3869±0.0081 | 26.2±0.6 | 26.5±0.6 |
| ex 7,8 | 19.86±1.74 | | | 0.2972±0.0059 | 1.3878±0.0082 | 26±0.6 | 26.3±0.6 |

| 3010 | U (ppm) | Th (ppb) | U/Th | $^{230}Th/^{238}U$ | $^{234}U/^{238}U$ | CS Age (ka) | Diff Age (ka) |
|---|---|---|---|---|---|---|---|
| 1 | 20.46 | 1624 | 13 | 0.3554±0.0341 | 1.3858±0.0324 | 31.9±3.6 | 32.4±3.6 |
| 2 | 17.88 | 22 | 832 | 0.3074±0.022 | 1.3871±0.0254 | 27±2.2 | 27.4±2.2 |
| 3 | 16.4 | 5 | 3332 | 0.324±0.0714 | 1.3856±0.0393 | 28.7±7.2 | 29.1±7.3 |
| 4 | 15.24 | 67 | 226 | 0.2851±0.0182 | 1.3789±0.0163 | 25±1.8 | 25.3±1.8 |
| 5 | 15.46 | 9 | 1789 | 0.2936±0.0152 | 1.3869±0.0204 | 25.7±1.5 | 26±1.5 |
| 6 | 14.19 | 13 | 1077 | 0.3022±0.0123 | 1.3827±0.0137 | 26.6±1.3 | 26.9±1.2 |
| 7 | 15.23 | 34 | 447 | 0.291±0.0173 | 1.3802±0.0162 | 25.6±1.7 | 25.9±1.7 |
| 8 | 13.55 | 75 | 180 | 0.3263±0.0108 | 1.3877±0.0178 | 28.9±1.2 | 29.3±1.1 |
| 9 | 8.67 | 79 | 110 | 0.3088±0.0228 | 1.3817±0.019 | 27.3±2.3 | 27.6±2.3 |
| 10 | 7.78 | 152 | 51 | 0.3172±0.0276 | 1.3888±0.0183 | 28±2.8 | 28.3±2.8 |

| | | | | | | | |
|---|---|---|---|---|---|---|---|
| 11 | 4.78 | 609 | 8 | 0.4316±0.0706 | 1.3725±0.0309 | 40.5±8 | 41.2±8.2 |
| 12 | 13.32 | 110 | 121 | 0.3088±0.0158 | 1.3913±0.0168 | 27.1±1.6 | 27.4±1.6 |
| 13 | 14.4 | 75 | 193 | 0.3113±0.0125 | 1.384±0.0126 | 27.5±1.3 | 27.8±1.3 |
| 14 | 13.83 | 458 | 30 | 0.3203±0.0168 | 1.392±0.016 | 28.2±1.7 | 28.6±1.7 |
| 15 | 3.62 | 532 | 7 | 0.1458±0.0368 | 1.3617±0.0254 | 12.3±3.3 | 12.4±3.3 |
| 16 | 2.92 | 1962 | 1 | 0.3715±0.1293 | 1.3072±0.0338 | 36±14.7 | 36.5±15.1 |
| **Mean Values** | | | | | | | |
| 1-16 | 12.36±2.61 | | | 0.3133±0.0095 | 1.3836±0.0097 | 27.7±1 | 28±1 |
| ex 1,11,15,16 | 13.83±1.68 | | | 0.3074±0.0096 | 1.3855±0.0097 | 27.1±1 | 27.4±1 |

**Table 2:** Lithogenic radionuclide data (Bq $kg^{-1}$) and calculated dose rates (Gy $ka^{-1}$) for OSL samples from Kiacatoo. All errors are 1σ.

| Sample | $^{238}U$ | $^{226}Ra$ | $^{210}Pb$ | $^{232}Th$ | $^{40}K$ | Measured water content (%) | Estimated long term average water content (%) | Cosmic D.R. (Gy $ka^{-1}$) | D.R. (Gy $ka^{-1}$)* |
|---|---|---|---|---|---|---|---|---|---|
| 1 | 26±3 | 27.6±0.6 | 18.4±2.0 | 34±2 | 342±5 | 18 | 10±5 | 0.20±0.02 | 2.13±0.17 |
| 2 | 35±2 | 28.5±0.5 | 29±2 | 41±2 | 396±5 | 16 | 10±5 | 0.20±0.02 | 2.58±0.21 |
| 3 | 29±4 | 32±1 | 28±3 | 40±2 | 445±7 | 17 | 10±5 | 0.20±0.02 | 2.67±0.21 |
| 4 | 31±3 | 33±2 | 29±4 | 44±3 | 422±9 | 21 | 10±5 | 0.20±0.02 | 2.68±0.22 |
| 5 | 32±2 | 35±1 | 34±2 | 46±1 | 487±5 | 21 | 10±5 | 0.20±0.02 | 2.98±0.23 |
| 6 | 31±4 | 37±1 | 47±4 | 47±2 | 515±9 | 19 | 10±5 | 0.20±0.02 | 3.25±0.26 |
| 7 | 33±1 | 27.8±0.4 | 25±1 | 38±1 | 400±3 | 8 | 12.5±5 | 0.19±0.02 | 2.41±0.19 |
| 8 | 34±2 | 27.2±0.6 | 29±2 | 52±3 | 505±6 | 15 | 12.5±5 | 0.17±0.02 | 2.96±0.24 |
| 9 | 28±2 | 25.1±0.4 | 29±2 | 42±1 | 385±6 | 11 | 12.5±5 | 0.13±0.01 | 2.41±0.19 |
| 10 | 7.3±1.3 | 8.3±0.2 | 12.6±1.1 | 11.1±0.7 | 400±4 | 2 | 12.5±5 | 0.16±0.02 | 1.69±0.11 |

*Internal dose rate of 0.03 ± 0.01 Gy/ka has been assumed.

**Table 3:** OSL data and age calculations for samples collected from Kiacatoo. All errors are 1σ.

| Sample | Lab Code | Accepted/ analysed grains | $\sigma_d$ (%) | k | $k_1$ prop (%) | $k_2$ prop (%) | $k_3$ prop (%) | $k_1$ De (Gy) | $k_2$ De (Gy) | $k_3$ De (Gy) | $k_1$ Age* (ka) | $k_2$ Age* (ka) | $k_3$ Age* (ka) |
|---|---|---|---|---|---|---|---|---|---|---|---|---|---|
| 1 | GU4.19 | 40/500 | 31±2 | 2 | 74±8 | 26±8 | | 38.5±1.4 | 77.1±7.4 | | 18 ± 2 | 36 ± 5 | |
| 2 | GU4.1 | 105/1000 | 26±1 | 3 | 45±12 | 41±13 | 14±4 | 56.3±2.9 | 74.8±3.5 | 36.2±1.8 | 22 ± 2 | 29 ± 3 | 14 ± 1 |
| 3 | GU4.20 | 50/500 | 46±2 | 2 | 78±6 | 23±6 | | 43.3±1.5 | 115.4±8.5 | | 16 ± 2 | 43 ± 5 | |
| 4 | GU4.2 | 51/500 | 28±1 | 2 | 72±11 | 28±11 | | 45.9±2.1 | 74.1±6.8 | | 17 ± 2 | 28 ± 4 | |
| 5 | GU4.21 | 43/500 | 35±2 | 2 | 62±14 | 38±14 | | 30.2±2.0 | 53.8±6.1 | | 10 ± 1 | 18 ± 3 | |
| 6 | GU4.3 | 60/500 | 21±1 | 2 | 55±16 | 45±16 | | 39.4±2.3 | 53.9±3.5 | | 12 ± 1 | 17 ± 2 | |
| 7 | GU4.6 | 71/1000 | 20±1 | 1 | 100 | | | 68.8±2.0 | | | 29 ± 3 | | |
| 8 | GU4.5 | 33/500 | 18±1 | 1 | 100 | | | 73.4±3.1 | | | 25 ± 3 | | |
| 9 | GU4.15 | 22/500 | 12±1 | 1 | 100 | | | 101.5±4.7 | | | 42 ± 4 | | |
| 10 | GU4.18 | 58/500 | 18±1 | 1 | 100 | | | 48.0±1.4 | | | 28 ± 2 | | |

*An additional 2 % systematic uncertainty has been included in the age uncertainty to account for possible bias in laboratory beta-source calibration. All ages and uncertainties rounded to nearest 1000 years.